Dawson Daniel M. (Orcid ID: 0000-0002-8110-4535)

Ashbrook Sharon E. (Orcid ID: 0000-0002-4538-6782)

Exploring Cation Disorder in Mixed-Metal Pyrochlore Ceramics using ^{17}O NMR Spectroscopy and First-Principles Calculations

Arantxa Fernandes,[1] Robert F. Moran,[1] David McKay,[1,2] Ben Griffiths,[1] Anna Herlihy,[1] Karl R. Whittle,[3] Daniel M. Dawson[1]* and Sharon E. Ashbrook[1]*

[1]*School of Chemistry, EaStCHEM and Centre of Magnetic Resonance, University of St Andrews, St Andrews KY16 9ST, UK.*

[2]*Current address: EPCC, University of Edinburgh, Bayes Building, 47 Potterrow, Edinburgh, EH8 9BT, UK.*

[3]*School of Engineering, University of Liverpool, Brownlow Hill, Liverpool, L69 3GH, UK.*

*Authors to whom correspondence should be addressed.

Email: *dmd7@st-andrews.ac.uk, sema@st-andrews.ac.uk.*

Submitted to *Magn. Reson. Chem.*

This article has been accepted for publication and undergone full peer review but has not been through the copyediting, typesetting, pagination and proofreading process which may lead to differences between this version and the Version of Record. Please cite this article as doi: 10.1002/mrc.5140

Abstract

Characterising the local structures (*e.g.*, the cation distribution) of mixed-metal ceramics by NMR spectroscopy is often challenging owing to the unfavourable properties (low γ, large quadrupole moment and/or low abundance) of many metal nuclei. ^{17}O is an attractive option owing to the prevalence of oxygen within ceramics. The moderate γ and small quadrupole moment of ^{17}O mean that the greatest barrier to accessing the information available from this nucleus is isotopic enrichment. We explore the challenges of ensuring uniform isotopic enrichment with $^{17}O_2(g)$ for the pyrochlore solid solutions, $Y_2Sn_xTi_{2-x}O_7$, $La_2Sn_xZr_{2-x}O_7$ and $La_2Sn_xHf_{2-x}O_7$, demonstrating that high enrichment temperatures (900 °C for 12 h) are required. In addition, for sites with very high symmetry (such as the tetrahedral OY4 and OLa4 sites with $C_Q \approx 0$ present here), we demonstrate that quantitative ^{17}O NMR spectra require correction for the differing contributions from the centreband of the satellite transitions, which can be as high as a factor of ~3.89. It is common to use first-principles calculations to aid in interpreting NMR spectra of disordered solids. Here, we use an ensemble modelling approach to ensure that all possible cation arrangements are modelled in the minimum possible number of calculations. By combining uniform isotopic enrichment, quantitative NMR spectroscopy and a comprehensive computational approach, we are able to show that the cation distribution in $Y_2Sn_xTi_{2-x}O_7$ is essentially random, whereas in $La_2Sn_xZr_{2-x}O_7$ and $La_2Sn_xHf_{2-x}O_7$, OLa2SnZr and OLa2SnHf sites are slightly energetically disfavoured, leading to a weak preference for clustering of like cations.

Introduction

Oxides play an important role in technology and industry, with applications in catalysis, as electrode materials, in the energy arena, as pigments and ceramics, and in the immobilization of radioactive waste.[1] The crystal chemical flexibility of oxide structures allows the fine tuning of their physical and chemical properties upon substitution of iso- or aliovalent ions. However, structural characterization of such disordered systems can be challenging; only information on the average structure is provided by techniques based on Bragg diffraction, but the local chemical structure has a significant impact on how a material behaves. Understanding the number and distribution of species within the crystal lattice is a vital step in understanding the structure-property relationship and, ultimately, in the future design of novel and improved functional materials. NMR spectroscopy provides an ideal tool for the characterisation of disordered solids,[2-4] with its sensitivity to the local environment, and the recent combination of experiment with computation (often referred to as NMR crystallography[5,6]) has facilitated the interpretation of the complex spectral lineshapes that are often encountered.

For oxides, oxygen NMR spectroscopy should be expected to be a useful (perhaps even routine) tool, potentially providing insight into the cation distribution in mixed-metal systems.[7,8] However, such measurements are limited by the low natural abundance of the only NMR-active isotope of O, ^{17}O (0.037%), while its high spin quantum number ($I = 5/2$) leads to spectra affected by second-order quadrupolar broadening, limiting both sensitivity and resolution. Solutions to the latter problem include the use of higher magnetic fields and two-dimensional approaches such as multiple-quantum MAS (MQMAS)[9] NMR experiments. In the former case, the easiest solution is isotopic enrichment.[8] However, this is typically very costly, often requiring the adaption of synthetic methods to ensure the

enrichment is cost effective and atom efficient, with recent work exploiting ionothermal synthesis, dry gel conversion reactions, solvent steaming, reversible small scale hydrolysis and mechanochemistry for enrichment of a range of inorganic solids.[10-15] Oxides are often enriched *via* post-synthetic exchange with $^{17}O_2(g)$,[7,8] but recent work on $A_2B_2O_7$ ceramics[16] has shown that care has to be taken over the choice of enrichment temperatures and times, both to mitigate preferential enrichment of chemically different O species, and to prevent any modification of the structure at high temperature.

Here, we explore the use of ^{17}O NMR spectroscopy to investigate the cation distribution in three mixed-metal pyrochlore solid solutions; $Y_2Sn_xTi_{2-x}O_7$, $La_2Sn_xZr_{2-x}O_7$ and $La_2Sn_xHf_{2-x}O_7$. For $Y_2Sn_xTi_{2-x}O_7$, ^{89}Y and ^{119}Sn (both I = 1/2) NMR spectroscopy have been used previously for structural characterization of $Y_2Sn_xTi_{2-x}O_7$.[17-23] MAS NMR experiments, first-principles calculations (and more recently ensemble-based modeling approaches[23]), revealed that the ^{89}Y and ^{119}Sn isotropic chemical shifts are sensitive to small changes in the local environment (in the number of Sn/Ti next nearest neighbours (NNN) and in their spatial arrangement). However, the resulting NMR spectra contain complex and overlapped resonances (particularly for ^{119}Sn), which cannot be easily be unambiguously decomposed, limiting quantitative analysis. Comparison of the experimental spectra to those simulated using an ensemble of all possible models suggested that the cation distribution was close to random; however, there was some evidence for low levels of clustering/ordering of like cations.[23] In principle, the large shift range of ^{17}O and the presence of both the chemical shielding and quadrupolar interactions should make this nucleus a sensitive probe of the local structure,[7,8] allowing (assuming quantitative measurements can be made) the composition and distribution of cations to be investigated. Periodic planewave density functional theory (DFT) calculations[24,25] (on a suite of disordered structural models) are used alongside ^{17}O

NMR experiments on isotopically enriched materials, to aid interpretation and assignment of the spectral signals and to provide insight into the origin of the changes in the NMR parameters that are observed. This complementary approach should offer new insight into disorder in these important materials and allow the evaluation of the value of such measurements to oxides more generally.

Methods

Synthesis and X-ray diffraction

Materials were prepared using a conventional mixed metal oxide process. Stoichiometric quantities of commercially available Y_2O_3 (Sigma Aldrich, 99%), La_2O_3 (Sigma-Aldrich 99.9%), SnO_2 (Sigma Aldrich, 99.9%), TiO_2 (Sigma-Aldrich 99%), ZrO_2 (Sigma-Aldrich 99%)

or HfO_2 (Sigma Aldrich, 99%) were heated at 800-850 °C for 10 h to dry, before being ball milled in ZrO_2 media (600 rpm) with acetone. After drying, the resultant required powders were pressed into pellets using a uniaxial press. $Y_2Sn_xTi_{2-x}O_7$ samples were prepared in a similar way to previous work,[23] being calcined at 1400 °C for 48 h at a rate of 5 °C min^{-1} before being cooled, reground and pressed into pellets before heating at 1400 °C for a further 48 h. For $La_2Sn_x(Zr,Hf)_{2-x}O_7$, samples were calcined at 1400 °C for 24 h at a rate of 10 °C min^{-1}, cooled, reground, pressed into pellets and heated at 1400 °C for a further 24 h.

Samples were studied by powder X-ray diffraction (PXRD) to determine phase purity using a PANalytical Empyrean Diffractometer, with $CuK_{\alpha 1}$ (λ = 1.540598 Å) radiation operating at 45 mA, and 40 kV, with an X'celerator linear detector. Patterns were collected over the 2θ range of 10° to 80°, with a step size of 0.02°, and step duration of 0.4 s per step (total experimental time 1-2 hours). For the end members,

patterns were compared with those from the ICSD. All mixed-metal materials were confirmed to be single phase pyrochlore using PXRD. See Supporting Information for further information.

Isotopic enrichment

Samples were enriched by condensing ~0.03 L of 70% $^{17}O_2$(g) (Cortecnet) into a pre-evacuated quartz vial containing ~0.20 g of oxide, before heating in a tube furnace at temperatures of 900 °C for 12 h (unless otherwise stated). A ramp rate of 5 °C min^{-1} was used for heating and cooling. No significant changes were seen in PXRD patterns after enrichment. Enrichment levels were estimated to be ~5-7% by comparison to NMR spectra of a sample of ^{17}O-enriched $Y_2Sn_2O_7$, determined in previous work[16] using secondary ion mass spectrometry to be enriched to 5%.

NMR spectroscopy

^{17}O NMR spectra were acquired using a Bruker Avance III 600 MHz spectrometer, equipped with a wide-bore 14.1 T magnet, at a Larmor frequency of 81.4 MHz. Powdered samples were packed into 3.2 mm thin-walled ZrO_2 rotors and rotated at 18-21 kHz, using a 3.2 mm HX probe. Spectra were acquired using a radiofrequency nutation rate, ν_1, of ~71 kHz, a pulse duration of 0.5 μs ($\pi/14$) and a recycle interval of 5 s (except where otherwise stated), and are the result of averaging between 1024 and 2048 transients. Chemical shifts are given in ppm relative to distilled H_2O(l). T_1 measurements were performed using a saturation recovery experiment (also with a short flip angle pulse), with a typical saturation train of 100 pulses separated by intervals of 10 ms. ^{17}O MQMAS spectra were acquired using a z-filtered pulse sequence[26] with ν_1 of ~71 kHz for the excitation and conversion pulses and a CT-selective (ν_1 of ~3 kHz) $\pi/2$ pulse. Spectra are shown after shearing and the δ_1 axis is referenced according to the convention in Ref. [27].

Fitting of the spectral lineshapes was carried out using the SOLA program (available within the Topspin software). Experimental intensities were compared to those in spectra simulated using the density matrix simulation program SIMPSON,[28] as described in Ref. [16]. Spectra were simulated at 14.1 T (under the experimental conditions described above) using detection operators of I_{1x} (*i.e.*, all single-quantum coherences from the central transition (CT) and satellite transitions (ST)) or I_{1c} (*i.e.*, only CT coherences), using 250 × 320 angles.

Calculations

Calculations were carried out using the CASTEP DFT code (version 8.0 or version 16.0),[24] employing the gauge-including projector augmented wave (GIPAW)[25] approach to reconstruct the all-electron wavefunction in the presence of a magnetic field. Calculations were performed using the GGA PBE functional,[29] with core-valence interactions described by ultrasoft pseudopotentials, and accounting for scalar relativistic effects using ZORA.[30,31] A planewave energy cutoff of 60 Ry (~816 eV) was used, and integrals over the first Brillouin zone were performed using a Monkhorst-Pack grid[32] with a reciprocal space grid spacing of 0.04 2π $Å^{-1}$. In the geometry optimisation all atomic coordinates and unit cell parameters were allowed to vary, with a geometry optimization energy tolerance of 1×10^{-5} eV per atom and an decreased electronic structure energy tolerance of 1×10^{-9} eV per atom, as discussed in more in detail in previous work.[23] For each solid solution, a complete set of 279 symmetry unique structural models (containing a total of 15624 unique O sites) was generated as described in Ref. [23], using the site occupancy disorder (SOD) program,[33] and the geometry of each model was then optimised using CASTEP. See the Supporting Information for more detail.

Diagonalisation of the absolute shielding tensor, $\boldsymbol{\sigma}$, yields the three principal components, σ_{11}, σ_{22} and σ_{33}, from which the isotropic shielding is given by $\sigma_{iso} = (\sigma_{11}$

+ σ_{22} + σ_{33})/3. The corresponding computed chemical shift tensor, $\boldsymbol{\delta}$, and isotropic chemical shift, δ_{iso}, can be determined from $\boldsymbol{\sigma}$ to aid comparison to experiment. The details of the referencing procedures used in this work are given in the Supporting Information. Diagonalisation of the electric field gradient tensor, **V**, gives the principal components V_{XX}, V_{YY} and V_{ZZ}, from which the magnitude of the quadrupolar interaction, $C_Q = eQV_{ZZ}/h$, and the asymmetry parameter, $\eta_Q = (V_{XX} - V_{YY})/V_{ZZ}$, can be determined. Q is the nuclear quadrupole moment, for which a value of 25.58 mb was used for ^{17}O.[34] The quadrupolar product is defined as $P_Q = C_Q(1 + \eta_Q^2/3)^{1/2}$.

Results and Discussion

As shown in Figure 1, the $A_2B_2O_7$ pyrochlore structure (space group *Fd*–3*m*) is based on a supercell of AO_2 fluorite, with the ordered removal of 1/8th of the oxygen anions.[35-37] In addition to an eight-coordinate A site and six-coordinate B site, this results in two crystallographically distinct O species; O1, coordinated by four A cations and O2, coordinated by two A and two B cations, which occupy the Wyckoff 8a and 48f sites, respectively. (Note, that in some pyrochlore crystal structures in the literature the definition of O1 and O2 is reversed, but here we follow the nomenclature used in Ref. [38]). A pyrochlore phase is formed when the ratio of the radii of the A and B cations (r_A/r_B) is between 1.46 and 1.78 (with defect fluorite and layered perovskite phases usually formed if the ratio is lower or higher, respectively).[35-37] The pyrochlore structure is able to incorporate a diverse range of elements, can tolerate both cation and anion disorder, and supports variable oxidation states, resulting in over 500 known synthetic compositions. Lanthanide and actinide pyrochlores are of particular interest for use in the safe long-term disposal of radioactive waste, and are often found as components within ceramic wasteforms such as Synroc.[39] Titanate pyrochlores exhibit high chemical durability,

while the substitution of elements such as Zr or Hf increases the resistance of the system to amorphization.[39] The ability to mix cations, and thus modify the properties of the pyrochlore materials, is key to the design of improved materials.

Figure 2 shows ^{17}O MAS NMR spectra of five pyrochlore end members, $Y_2Sn_2O_7$, $Y_2Ti_2O_7$, $La_2Sn_2O_7$, $La_2Zr_2O_7$ and $La_2Hf_2O_7$, isotopically enriched in ^{17}O at 700 °C for 12 h. All show two distinct O signals, corresponding to O1 and O2 sites, and the NMR parameters extracted are given in Table 1. Also shown in Table 1 are the NMR parameters predicted from DFT calculations. Spectra for $Y_2Sn_2O_7$, $Y_2Ti_2O_7$ and $La_2Sn_2O_7$ are in good agreement with those in the previous literature.[16,40] By symmetry, the C_Q for O1 in all structures should be zero (reflecting the –43*m* point symmetry at the 8a site), although very small quadrupolar couplings are observed experimentally (extracted by fitting the ST sideband manifold in a slow MAS spectrum[16]), resulting from defects and/or surface effects, as discussed previously.

For the La-containing pyrochlores, the O1 signal is broader, with a complex and asymmetric lineshape seen upon expansion (see Supporting Information). As shown previously for $La_2Sn_2O_7$,[16] this is thought to result from the presence not only of a J coupling to four equivalent ^{139}La (I = 7/2, 99.9% abundance) nuclei, but also to the existence of a quadrupolar-dipolar cross term (or residual dipolar coupling).[41,42] This second-order interaction, resulting from a dipolar coupling to a nucleus with a very large C_Q, cannot be removed by MAS, owing to its more complex angular dependence. As shown in the Supporting Information, ^{139}La C_Q values for $La_2Zr_2O_7$ and $La_2Hf_2O_7$ (obtained from wideline NMR experiments[43] and supported by DFT calculations) are slightly larger (~87 MHz) than that previously observed for $La_2Sn_2O_7$ (~79 MHz), confirming a similar cross term is likely to be present, perturbing the intensities and spacings of the J multiplet. For O2, larger C_Q values are predicted by DFT calculations (ranging from 0.6 to 3.8 MHz), reflecting the lower

symmetry of this site (and its OA2B2 coordination environment). Good agreement is also observed with the experimental values (and where it exists, with previous literature[16,40]). It is noticeable, however, that when B = Sn (*i.e.*, $Y_2Sn_2O_7$ and $La_2Sn_2O_7$) the C_Q is considerably larger (~3.3 MHz experimentally) than when B = Zr, Hf or Ti (0.7-1.5 MHz).

Figure 3 shows ^{17}O MAS NMR spectra of three mixed-metal pyrochlore solid solutions; $Y_2Sn_xTi_{2-x}O_7$, $La_2Sn_xZr_{2-x}O_7$ and $La_2Sn_xHf_{2-x}O_7$. Samples were enriched at 900 °C for 12 hours. In all three cases, additional resonances are seen when compared to the respective end members, confirming the formation of mixed-metal materials. Signals at ~290 ppm, ~390 ppm and ~350 ppm can be tentatively assigned to OY2SnTi, OLa2Zr2 and OLa2Hf2 environments, respectively. Note that as substitution is thought only to occur at the B site, this affects the local coordination of only the O2 site (OA2B2), and not that of O1 (OA4), meaning that local environments such as OA3B and OAB3 *etc.*, will not occur unless antisite disorder is present.

The assignment of the additional signals seen experimentally can be confirmed by DFT calculations on a suite of structural models of all possible atomic arrangements of B site cations in a pyrochlore unit cell (see Supporting Information). For $Y_2Sn_xTi_{2-x}O_7$,[23] as shown in Figure 4a, DFT calculations predict isotropic chemical shifts of 260-340 ppm for the range of OY2SnTi environments seen throughout the solid solution, with predicted C_Q values between 2.5 and 3.1 MHz. While the shifts are in good agreement with the new signal seen in the experimental ^{17}O MAS NMR spectra, it is difficult to determine C_Q experimentally owing to the additional broadening arising from the distribution of NMR parameters that results from the increased disorder. However, information on the average P_Q and δ_{iso} values can be obtained the centre-of-gravity of the signal in an MQMAS spectrum. As shown in

the Supporting Information, for Y_2SnTiO_7, this gave $\langle P_Q \rangle$ and $\langle \delta_{iso} \rangle$ of ~2.4 MHz and ~300 ppm, respectively, in reasonable agreement with the predicted values. Calculated NMR parameters for OY4, OY2Sn2 and OY2Ti2 species in mixed-metal materials are also in good agreement with the experimental results.

As shown in Figure 3, there are small changes in the position of the ^{17}O resonances as a function of composition, resulting from changes in both δ_{iso} and C_Q, as shown in the Supporting Information. Experimentally, for $Y_2Sn_xTi_{2-x}O_7$, relatively little change in shift is seen for O1 (OY4), although for the mixed-metal materials this signal is significantly broader, with a range of δ_{iso} values predicted by DFT. The lowering of symmetry upon cation substitution also results in a non-zero C_Q in many cases. Although, in principle, this will also lead to increased broadening, this is small in comparison to the distribution of δ_{iso} (typically ~0.6 ppm at 14.1 T for C_Q = 0.6 MHz). As shown in the Supporting Information, for the three types of O2 species seen in mixed-metal materials, significant ranges of δ_{iso} and C_Q are predicted (particularly for OY2Ti2 and OY2SnTi), explaining the broadened lineshapes seen experimentally, and the lack of features characteristic of quadrupolar broadening. As shown in the histograms in the Supporting Information for Y_2SnTiO_7, the range of shifts seen is in good agreement with the width of the lineshapes seen in the experimental ^{17}O MAS NMR spectra, suggesting it is this distribution that dominates the spectrum. This is also in good agreement also with the ^{17}O MQMAS spectrum of Y_2SnTiO_7 shown in the Supporting Information, where significant broadening is observed along the axis (+17/31) associated with a distribution of chemical shifts.

For $La_2Sn_xZr_{2-x}O_7$ and $La_2Sn_xHf_{2-x}O_7$, the calculated δ_{iso} and C_Q values (shown in Figures 4b and 4c, respectively) confirm the assignment of the OLa_2SnZr and OLa_2SnHf O2 species (with average calculated values of 315 ppm/3.2 MHz and 276 ppm/3.1 MHz, respectively). In general, smaller ranges of calculated parameters are

seen as a function of composition for both materials relative to $Y_2Sn_xTi_{2-x}O_7$, (see Supporting Information), leading to lineshapes with features more characteristic of quadrupolar broadening for the sites with larger C_Q. Experimentally, the most significant change in δ_{iso} is seen for O1 (OLa4), where an increase in shift is observed with increasing Sn content (as shown in Figure 3). This is supported by the DFT calculations (see Supporting Information), which show a shift increase (but relatively little shift distribution) for O1 in both $La_2Sn_xZr_{2-x}O_7$ and $La_2Sn_xHf_{2-x}O_7$. Interestingly, for all O2 species, δ_{iso} decreases with increasing Sn content, although larger distributions of shift are seen. For the quadrupolar interaction, the lowering of the O1 point symmetry in the mixed-metal compounds again leads to non-zero C_Q values. However, these are still very small (~0.1 MHz) and considerably smaller than the corresponding values seen in $Y_2Sn_xTi_{2-x}O_7$. The larger C_Q values predicted for OLa2SnZr and OLa2SnHf species (3.2/3.1 MHz) are also seen experimentally, where $\langle P_Q \rangle$ values of ~2.7 and ~2.6 MHz can be extracted from ^{17}O MQMAS NMR spectra (as shown in the Supporting Information).

In principle, the relative amounts of each type of O species present can be determined from the integrated intensities of the signals in the ^{17}O MAS NMR spectra, potentially providing insight into the cation distribution. However, in practice, this requires uniform enrichment of the chemically different O species and the acquisition of quantitative NMR spectra, the latter being potentially challenging for quadrupolar nuclei such as ^{17}O. Previous work on ^{17}O NMR of $A_2B_2O_7$ materials (including $Y_2Sn_2O_7$, $Y_2Ti_2O_7$ and $La_2Sn_2O_7$)[16] showed that uniform relative enrichment of O1 and O2 sites was only achieved at higher enrichment temperatures or longer enrichment times. For the pyrochlore end members studied, preferential enrichment of O2 was observed for enrichment temperature below ~850 °C (for 12 h heating). Although significant changes in spectral intensities were seen with longer heating times at 600 °C, uniform relative enrichment was not observed at this

temperature for all end members even after 96 h. Possible origins for this observation were suggested to be the difference in bond strengths between O1 (surrounded only by A cations) and O2 (surrounded by 2 A and 2 B cations), or differences arising from the mechanism of enrichment (including the ability to create split vacancies) as proposed by prior computational work.[44-46] For $La_2Zr_2O_7$ and $La_2Hf_2O_7$ (which were not studied in the original work), ^{17}O enrichment was carried out in this work at a variety of temperatures and times. The resulting ^{17}O MAS NMR spectra reveal that for both materials the overall signal intensity increases as the enrichment temperature is raised, with higher levels of ^{17}O incorporated. Preferential enrichment of O2 is seen at the lowest temperatures, with an approximately constant O1 : O2 ratio observed above ~700 °C (for 12 h heating), in good agreement with the previous results for other pyrochlore end members.[16] At 500 °C, a similar O1 : O2 ratio is not observed even with much longer heating times (up to 72 h for $La_2Hf_2O_7$). As an example of a mixed-metal material, Figure 5 shows ^{17}O MAS NMR spectra of Y_2SnTiO_7, enriched for 12 h at 600 °C, 700 °C and 900 °C. Each O2 species (*i.e.*, OY2Ti2, OY2Sn2 and OY2SnTi) has a similar absolute level of enrichment at the three temperatures, but there is a significant increase in the relative level of enrichment of O1 between 600 °C and 700 °C (with little additional change on moving to 900 °C). To ensure the most uniform relative enrichment of all O species in all mixed-metal materials, therefore, enrichment of mixed-metal materials was carried out at 900 °C for 12 h.

For the end member pyrochlores, the theoretical O1 : O2 ratio is 1 : 6, reflecting the Wyckoff 8a and 48f positions. For mixed metal materials there are three types of O2 present in the disordered system (OA2B2, OA2BB' and OA2B'2), but a ratio of 1 : 6 (0.1667) would still be expected when all O2 sites were considered together. This, however, is not what is seen experimentally. Figure 6 plots the integrated O1/O2 ratios (black points), extracted from the ^{17}O MAS NMR spectra of $Y_2Sn_xTi_{2-x}O_7$,

$La_2Sn_xZr_{2-x}O_7$ and $La_2Sn_xHf_{2-x}O_7$ in Figure 3. The ratios are relatively constant as a function of composition, suggesting the temperature of enrichment is sufficient to ensure consistent relative enrichment of all chemically distinct species. However, O1/O2 is 0.4-0.5 for $Y_2Sn_xTi_{2-x}O_7$ and ~0.6 for $La_2Sn_xZr_{2-x}O_7$ and $La_2Sn_xHf_{2-x}O_7$, rather than the 0.1667 expected. As ^{17}O is quadrupolar, the relative spectral intensities need to be corrected for any differences in nutation for species with different quadrupolar couplings, and for any contribution of the STs to the CT centreband. Furthermore, any differences in T_1 relaxation between different sites would also need to be accounted for to ensure quantitative spectral acquisition.

Saturation recovery experiments were performed to measure T_1 times for the pyrochlore end members, with results given in Table 2. A very wide range of T_1 values are seen, with notably smaller values (*i.e.*, faster relaxation) for the La-based materials. This perhaps reflects the presence of the high-γ, high abundance, quadrupolar ^{139}La cation on the A sites (and so directly bound to both O species), rather than the low-γ, spin I = 1/2 ^{89}Y cation present on the A site in $Y_2Sn_2O_7$ and $Y_2Ti_2O_7$. Table 2 shows that for fully quantitative spectra to be obtained a very long recycle interval would be required (*e.g.*, 5 T_1 for O1 in $Y_2Sn_2O_7$ is ~1800 s). In order to avoid this problem, spectra were acquired using a shorter recycle interval (5 s) and corrected for the relative differences in relaxation of all species.

In order to ensure that any differences in nutation and any contributions of the ST are correctly taken into account, accurate C_Q values must be obtained. As described earlier this can be challenging experimentally (if characteristic quadrupolar lineshapes are not observed), but the magnitude of the quadrupolar interaction can be estimated either by fitting the ST sideband manifold (when C_Q is small) or from the position of resonances in MQMAS experiments (when lineshapes are broadened by disorder). Simulations using SIMPSON[28] (shown in the Supporting Information)

reveal that there are no differences in relative excitation efficiency for species with C_Q values up to 3.2 MHz for the short flip angles used in the spectral acquisition (formally $\pi/14$). However, when C_Q is very small, some of the signal intensity attributed to the CT in experimental spectra actually results from the centreband of the STs.[2,3,16] As C_Q increases, the increasingly diverging second-order isotropic quadrupolar shifts of the STs and CT ensure that these signals are separated overlap, hence enabling integrated intensities of signals to be unambiguously determined. The ST contribution to any signal can be predicted from density matrix simulations and relative spectral intensities corrected accordingly, as shown in the Supporting Information for Y_2SnTiO_7. The O1/O2 ratios, corrected both for T_1 differences and ST contributions, are shown by the red axis in Figure 6, for all three series. After corrections have been applied, all ratios are much closer to the theoretical value of 0.1667, suggesting uniform relative enrichment is obtained under the experimental conditions chosen. It is interesting to note that there is a larger variation (both before, but particularly after, correction) for $Y_2Sn_xTi_{2-x}O_7$. This reflects the need to apply significant corrections to both the O1 and the O2 OY2Ti2 signals for this series (unlike $La_2Sn_xZr_{2-x}O_7$ and $La_2Sn_xHf_{2-x}O_7$ where a significant correction is only applied to O1), and the much greater variation in the quadrupolar parameters predicted by DFT as the composition varies (see Figure 4). This would lead, in principle, to a greater variation in the correction factors required, and so a larger error when applied to the experimental (summed) signal.

Once the relative spectral intensities have been corrected as described above, it is possible to compare these to the intensities that would be obtained should the B cations be distributed completely randomly. For O2, it can be shown using simple statistics that the probability of finding n Sn neighbours is $P(n\ Sn) = \Omega (x/2)^n (1 - (x/2))^{2-n}$, where Ω is the number of possible permutations and x is taken from the formula. These probabilities are plotted, with the experimental values for $Y_2Sn_xTi_{2-}$

$_xO_7$, $La_2Sn_xZr_{2-x}O_7$ and $La_2Sn_xHf_{2-x}O_7$, in Figure 7. All three show good agreement between experimental data and predicted intensities, suggesting that the B site cation distribution is close to random in all. For $Y_2Sn_xTi_{2-x}O_7$, this is consistent with previous work using ^{89}Y and ^{119}Sn NMR spectroscopy.[23] Agreement between experimental spectra and spectra simulated using NMR parameters calculated from an ensemble of structural models was better at higher temperatures, indicating all atomic arrangements were likely to contribute equally, *i.e.*, suggesting a random distribution of B site cations. Small deviations between the experimental and simulated spectra were noted for the less substituted materials, but while these were potentially attributed to a weak preference for clustering or ordering, it was shown they could also result from the limitations of using a single unit cell in the ensemble-based modelling.[23] The overlap of the signals in the ^{89}Y and ^{119}Sn NMR spectra make it impossible to easily determine the relative intensities of specific spectral signals and necessitates a comparison of the whole spectrum to evaluate (qualitative) agreement between experiment and theory. However, as shown in Figure 3, the good spectral resolution between chemically different O2 species in the ^{17}O NMR spectra allows (after corrections have been applied) the straightforward extraction of relative intensities and an easy comparison to theory.

The good agreement seen in Figure 7a suggests a random distribution of B site cations is present for $Y_2Sn_xTi_{2-x}O_7$, with no evidence for any substantial clustering or ordering. The plots for $La_2Sn_xZr_{2-x}O_7$ and $La_2Sn_xHf_{2-x}O_7$ in Figures 7b and 7c, respectively, also show good agreement between the experimental data and theoretical predictions, but in both cases the deviation between the two is greater than for $Y_2Sn_xTi_{2-x}O_7$, with a small underestimation of OLa2SnX (where X = Zr of Hf) relative to OLa2Sn2 and OLa2X2, across much of the compositional range. This could suggest there is a weak preference for clustering, with the substitution of two like cations (*i.e.*, Sn2 or X2) preferred over the mixed (SnX) substitution. For each composition studied, a complete set of structural models (*i.e.*, all possible B site

cation arrangements within a single unit cell) have been generated, and so it is possible to consider whether there is any significant difference in energy between models with a more random distribution of Sn and Zr/Hf cations (*i.e.*, with more OLa2SnX, where X = Zr or Hf) and those exhibiting clustering of like cations (*i.e.*, with more OLa2Sn2 and OLa2X2 species). As an example, Figure 8 plots of the enthalpy of mixing (ΔH_{mix}) for a particular structural model against the number of O2 OA2BB' species (*i.e.*, OY2SnTi, OLa2SnZr and OLa2SnHf) for the x = 1 compositions of each series. (Full data for all compositions is given in Figure S5.7 in the Supporting Information). For La_2SnZrO_7 and La_2SnHfO_7, a correlation is clearly seen, with those models having fewer of these species (and therefore more OLa2Sn2 and OLa2X2) having lower energy (by ~8-9 meV/O atom). This suggests that there is a small preference for local clustering of like cations in these two solid solutions. Interestingly, for $Y_2Sn_xTi_{2-x}O_7$, very little correlation between the number of OY2SnTi species and mixing enthalpy is seen, confirming a more random cation distribution is expected, in good agreement with the experimental results in Figure 7a.

One significant advantage of an NMR crystallographic approach that combines experiment and computation is the possibility to gain additional insight into the origin of the NMR parameters and their detailed dependence on the atomic-scale environment. Figures 9 and 10 show how the ^{17}O NMR parameters (δ_{iso} and C_Q) vary with changes to the local geometry (including the average O-X bond length, $\langle r_{O\text{-}X} \rangle$, the distortion index, DI,[7] and the average electronegativity of the neighbouring cations, $\langle \chi_X \rangle$. Figure 9a shows that in most cases there is very little variation in $\langle r_{O\text{-}X} \rangle$ and DI for a particular type of O species (although these parameters vary significantly between chemically different O), and little correlation more generally with δ_{iso}. However, larger variation in both $\langle r_{O\text{-}X} \rangle$ and DI is observed for all O species in $Y_2Sn_xTi_{2-x}O_7$, with particularly large changes seen for OY2Ti2, with increases in

both parameters resulting in an increase in ^{17}O δ_{iso}. These substantial changes to the local geometry (not seen for $La_2Sn_xZr_{2-x}O_7$ and $La_2Sn_xHf_{2-x}O_7$) result from the size mismatch in the B site cations (with ionic radii of 0.69 Å for Sn^{4+} and 0.61 Å for Ti^{4+}, compared to 0.72 Å and 0.71 Å for Zr^{4+} and Hf^{4+}).[47] Previous work[23] showed that it is energetically less favourable to substitute the smaller Ti^{4+} cation into $Y_2Sn_2O_7$ than *vice versa*, with this cation too small to satisfy the bonding requirements of all surrounding oxygens, leading to significant distortions of the local environment and a wide distribution of Ti-O bond lengths.

Figure 9c shows a reasonable correlation between ^{17}O δ_{iso} and $\langle\chi_X\rangle$, with an increase in $\langle\chi_X\rangle$ leading to a decrease in δ_{iso}. This is in contrast to the conclusion in Ref. [8], where it was shown that there was little correlation between ^{17}O δ_{iso} and $\langle\chi_X\rangle$. However, this earlier work compiled many results for general X-O-X bonding arrangements for a wide variety of materials, where much greater structural variation is present. The structural similarity of the pyrochlore systems considered here (which all have similar numbers and arrangements of the surrounding atoms for each type of O site) allows the dependence of δ_{iso} on $\langle\chi_X\rangle$ to be more clearly revealed. (It should be noted that the largest deviations from the line of best fit are for O species that are coordinated by Ti^{4+}, likely reflecting the larger structural distortions seen in these materials, as discussed above). The dependence of δ_{iso} on $\langle\chi_X\rangle$ allows shifts for environments such as OA3B, OAB3, *etc*., which would result from antisite mixing (*i.e.*, A cations occupying B sites within the structure and *vice versa*) to be predicted. Signals at these shifts are clearly not seen in the experimental spectra, suggesting that such mixing is not present (at least at levels observable at these signal-to-noise ratios).

As noted above, very different ^{17}O C_Q values are observed for the chemically different O2 species, with those that are coordinated by Sn usually much greater

(typically 3-4 MHz) than those that are not (typically 0-1 MHz). Notably, O2 ^{17}O C_Q values for OY2Sn2 and OLa2Sn2 species are larger than those for the arguably less symmetrical OY2SnTi, OLa2SnZr and OLa2SnHf environments. Figure 10 reveals this difference does not stem from any significant difference in the arrangement of neighbouring cations, with very similar $\langle r_{O\text{-}X} \rangle$ and DI for all O2 environments in each of the Y- and La-based materials, respectively. Instead, it is likely the differences in C_Q results from significantly increased covalency of the Sn-O bond, leading to more directional bonding and an amplification of the electric field gradient. The dependence of ^{17}O C_Q on $\langle \chi_X \rangle$, which can be viewed as a proxy for ionicity/covalency, is shown in Figure 10c, with an increase in $\langle \chi_X \rangle$ leading to an increased C_Q. This is in good agreement with the conclusions for previous work considering a wide range of O-containing compounds, which showed a correlation between C_Q and the average ionicity, I, of the O-M bonds (with C_Q (in MHz) = – 0.203 I(%) + 14.78).[8] As the electronegativity of the coordinated cations increases (*i.e.*, is closer to that of O) there is an increase in covalency and a decrease in ionicity, leading to an increased C_Q.

Conclusions

In this work, we have combined isotopic enrichment, quantitative ^{17}O NMR spectroscopy and first-principles calculations on a suite of structures resulting from ensemble-based modelling, in an NMR crystallographic approach to investigating cation disorder in pyrochlore ceramics. Although the quadrupolar nature of ^{17}O (I = 5/2) offers advantages, with both the shielding and quadrupolar parameters able to distinguish between different O species and providing additional detail on the local structure, this also poses challenges for extracting accurate and quantitative information, while the low γ and low natural abundance hinders sensitivity. We have shown that mixed-metal pyrochlores can be uniformly enriched post synthesis,

by exchange with $^{17}O_2$ gas, but that high temperatures (800-900 °C) are required to ensure this enrichment is uniform between distinct O species. Quantitative ^{17}O NMR spectra can be acquired using pulses with short flip angles to minimize any differences in nutation behaviour between sites with different C_Q. However, it is also vital to correct spectral intensities both for any differences in relative T_1 relaxation rates (which can be very long for some O species in oxides) and (for species with very low C_Q) to account for any contribution of the centreband of the STs to the CT signal. This correction (determined here using density matrix simulations) requires a knowledge of the quadrupolar coupling which is not always straightforward to extract if little second-order broadening is seen or if lines are inhomogeneously broadened by the distribution of NMR parameters arising from disorder. Information on C_Q can be obtained through experiments (from the ST sideband manifolds or from MQMAS spectra) but can also be determined using first-principles calculations. Here, we exploit an ensemble-based modelling approach that allows us to generate all possible atomic arrangements for a specific composition, while ensuring symmetry-related models are not considered, minimising the computational cost. The predicted NMR parameters help to assign and interpret the spectral lineshapes obtained.

The ^{17}O NMR spectra of the pyrochlore solid solutions show good resolution of chemically different oxygens, allowing straightforward and accurate integrated spectral intensities to be determined (in contrast to the overlapped spectral lineshapes seen for ^{89}Y and ^{119}Sn NMR spectra in previous work on one of the systems studied). These intensities can then be compared to those expected from the probability of finding different atomic arrangements if the distribution of B site cations was completely random (obtained from simple statistics). Good agreement is found for $Y_2Sn_xTi_{2-x}O_7$, while for $La_2Sn_xZr_{2-x}O_7$ and $La_2Sn_xHf_{2-x}O_7$ the results suggest that while a random distribution of B site cations is present, there is also a weak

preference for the clustering of like cations (*i.e.*, with an increase in the intensities of OLa2Sn2 and OLa2X2 environments at the expense of OLa2SnX). This conclusion is supported by the DFT calculations, which show a correlation between the lower energy of a structural model and the lower number of mixed metal OLa2SnX environments. Such a clear correlation is not observed for $Y_2Sn_xTi_{2-x}O_7$, explaining the observation of a more random cation distribution in these materials, most likely owing to the more significant structural distortions present as a result of the greater size mismatch between the B site cations. We show that both the ^{17}O isotropic chemical shift and quadrupolar coupling depend on the average electronegativity of the coordinated cations. In the former case, this provides additional support for the lack of any signals resulting from antisite disorder (*i.e.*, the substitution of B cations onto A sites and *vice versa*). In the latter, larger C_Q values are seen for O species that are coordinated by Sn. This does not result from any distortion in the local structures but from the increased covalency of the Sn-O bond.

Despite the challenges of enrichment and quantitative spectral acquisition, ^{17}O NMR has great potential in the study of atomic-scale structure and disorder in ceramics. In many cases, ^{17}O may be the only feasible option for study, particularly when metals with very low receptivity or very large quadrupole moments, such as ^{91}Zr, $^{177/179}Hf$ and ^{139}La, are present. The large shift resolution seen for chemically different O species will also be an advantage when studying more complex systems (*e.g.*, with substitution of multiple cations onto multiple crystallographically distinct sites). The complementary application of experiments and computation is clearly advantageous in assigning ^{17}O spectra and interpreting and analysing the results obtained. When combined with information from other multinuclear NMR experiments (where possible) and from diffraction and/or microscopy, ^{17}O NMR spectroscopy should be considered as a vital tool in the arsenal of the chemist for

providing a detailed structural picture of a material over different lengthscales and timescales.

Acknowledgements

We are grateful to EPSRC for support through the Collaborative Computational Project on NMR Crystallography (CCP-NC), *via* EP/M022501/1, and to the ERC (EU FP7 Consolidator Grant 614290 "EXONMR"). SEA would also like to thank the Royal Society and Wolfson Foundation for a merit award. Ricardo Grau-Crespo (University of Reading) is thanked for useful discussions. The research data (and/or materials) supporting this publication can be accessed at DOI: XXXXX.[48]

Table 1. Experimental and calculated ^{17}O NMR parameters (isotropic chemical shift, δ_{iso}, quadrupolar coupling constant, C_Q, and asymmetry parameter, η_Q) for $Y_2Sn_2O_7$, $Y_2Ti_2O_7$, $La_2Sn_2O_7$, $La_2Zr_2O_7$ and $La_2Hf_2O_7$ pyrochlores.

		Experiment			Calculation		
Composition	O site	δ_{iso} (ppm)	C_Q / MHz	η_Q	δ_{iso}^{calc} (ppm)	$\lvert C_Q \rvert^{calc}$ / MHz	η_Q^{calc}
$Y_2Sn_2O_7$	O1	384.0 (5)	~0.02 (2)	n.d.[a]	388.2[a]	0.0[b]	-
	O2	172.5 (5)	3.2 (1)	0.4 (1)	174.9[a]	3.52[b]	0.35[b]
$Y_2Ti_2O_7$	O1	386.1 (5)	~0.02 (2)	n.d.[a]	374.5[a]	0.0[b]	-
	O2	454.6 (5)	0.7 (1)	0.5 (1)	459.6[a]	0.64[b]	0.75[b]
$La_2Sn_2O_7$	O1	641.5 (5)	~0.02(2)	n.d.[a]	631.0[b]	0.0[c]	-
	O2	222.0 (5)	3.3 (1)	0.9 (1)	208.5[b]	3.79[c]	0.99[c]
$La_2Zr_2O_7$	O1	626.3 (5)	~0.02(2)	n.d.[a]	622.9[b]	0.0[c]	-
	O2	394.0 (5)	1.5 (1)	0.4 (1)	421.5[b]	1.08[c]	0.98[c]
$La_2Hf_2O_7$	O1	629.9 (5)	~0.02(2)	n.d.[a]	626.3	0.0[c]	-
	O2	350.8 (5)	1.4 (1)	0.6 (1)	343.8[b]	1.03[c]	0.58[c]

[a]n.d. = not determined. [b] CASTEP version 8.0, [c] CASTEP version 16.0

Table 2. ^{17}O T_1 relaxation time constants (measured using saturation recovery experiments) for the pyrochlore end members.

Composition	O site	T_1 / s
$Y_2Sn_2O_7$[16]	O1	367 (5)
	O2	295 (5)
$Y_2Ti_2O_7$[16]	O1	230 (5)
	O2	71 (3)
$La_2Sn_2O_7$[16]	O1	12 (2)
	O2	17 (2)
$La_2Zr_2O_7$	O1	7 (2)
	O2	9 (2)
$La_2Hf_2O_7$	O1	5 (2)
	O2	5 (2)

References

[1] M. Lorenz, M. S. Ramachandra Rao, T. Venkatesan, E. Fortunato, P. Barquinha, R. Branquinho, D. Salgueiro, R. Martins, E. Carlos, A. Liu, F. K. Shan, M. Grundmann, H. Boschker, J. Mukherjee, M. Priyadarshini, N. DasGupta, D. J. Rogers, F. H. Teherani, E. V. Sandana, P. Bove, K. Rietwyk, A. Zaban, A. Veziridis, A. Weidenkaff, M. Muralidhar, M. Murakami, S. Abel, J. Fompeyrine, J. Zuniga-Perez, R. Ramesh, N. A. Spaldin, S. Ostanin, V. Borisov, I. Mertig, V. Lazenka, G. Srinivasan, W. Prellier, M. Uchida, M. Kawasaki, R. Pentcheva, P. Gegenwart, F. Miletto Granozio, J. Fontcuberta, N. Pryds *J. Phys. D* **2016**, *49*, 43.

[2] S. E. Ashbrook, D. M. Dawson, J. M. Griffin, *Solid-State NMR Spectroscopy* in: *Local Structural Characterisation*, D.W. Bruce, D. O'Hare, R.I. Walton (Eds.), John Wiley & Sons Ltd, Chichester, **2014**.

[3] D. C. Apperley, R. K. Harris, P. Hodgkinson, Solid State NMR Basic Principles and Practice, Momentum Press, New York, **2012**.

[4] R. F. Moran, D. M. Dawson, S. E. Ashbrook, *Int. Rev. Phys. Chem.* **2017**, *36*, 39.

[5] C. Bonhomme, C. Gervais, F. Babonneau, C. Coelho, F. Pourpoint, T. Azais, S. E. Ashbrook, J. M. Griffin, J. R. Yates, F. Mauri, C. J. Pickard, *Chem. Rev.* **2012**, *112*, 5733.

[6] S. E. Ashbrook, D. McKay, *Chem. Commun*. **2016**, *52*, 7186.

[7] K. J. D. MacKenzie, M. E. Smith, Multinuclear Solid-State NMR of Inorganic Materials. Pergamon, Oxford, UK, **2002**.

[8] S. E. Ashbrook, M. E. Smith, *Chem. Soc. Rev.* **2006**, *35*, 718.

[9] L. Frydman, J. S. Harwood, *J. Am. Chem. Soc*. **1995**, *117*, 5367.

[10] J. M. Griffin, L. Clark, V. R. Seymour, D. W. Aldous, D. M. Dawson, D. Iuga, R. E. Morris, S. E. Ashbrook, *Chem. Sci*. **2012**, *3*, 2293.

[11] P. He, J. Xu, V. V. Terskikh, A. Sutrisno, H.-Y. Nie, Y. Huang, *J. Phys. Chem. C* **2013**, *117*, 16953.

[12] G. P. M. Bignami, Z. H. Davis, D. M. Dawson, S. A. Morris, S. E. Russell, D. McKay, R. E. Parke, D. Iuga, R. E. Morris, S. E. Ashbrook, *Chem. Sci.* **2018**, *9*, 850.

[13] A. Flambard, L. Montagne, L. Delevoye, *Chem. Commun*. **2006**, 3426.

[14] S. M. Pugh, P. A. Wright, D. J. Law, N. Thompson, S. E. Ashbrook, *J. Am. Chem. Soc.* **2020**, *142*, 900.

[15] T.-X. Metro, C. Gervais, A. Martinez, C. Bonhomme and D. Laurencin, *Angew. Chem.* **2017**, *129*, 6907.

[16] A. Fernandes, R. F. Moran, S. Sneddon, D. M. Dawson, D. McKay, G. P. M. Bignami, F. Blanc, K. R. Whittle, S. E. Ashbrook, *RSC Adv*. **2018**, *8*, 7089.

[17] C. P. Grey, C. M. Dobson, A. K. Cheetham, R. J. B. Jakeman, *J. Am. Chem. Soc*. **1989**, *111*, 505.

[18] C. P. Grey, M. E. Smith, A. K. Cheetham, C. M. Dobson, R. Dupree, J. *Am. Chem. Soc.* **1990**, *112*, 4670.

[19] S. E. Ashbrook, K. R. Whittle, G. R. Lumpkin, I. Farnan, *J. Phys. Chem. B* **2006**, *110*, 10358.

[20] S. W. Reader, M. R. Mitchell, K. E. Johnston, C. J. Pickard, K. R. Whittle, S. E. Ashbrook, *J. Phys. Chem. C* **2009**, *113*, 18874.

[21] M. R. Mitchell, S. W. Reader, K. E. Johnston, C. J. Pickard, K. R. Whittle, S. E. Ashbrook, *Phys. Chem. Chem. Phys.* **2011**, *13*, 488.

[22] M. R. Mitchell, D. Carnevale, R. Orr, K. R. Whittle, S. E. Ashbrook, J. *Phys. Chem. C* **2012**, *116*, 4273.

[23] R. F. Moran, D. McKay, P. C. Tornstrom, A. Aziz, A. Fernandes, R. Grau-Crespo, S. E. Ashbrook, J. *Am. Chem. Soc.* **2019**, *141*, 17838.

[24] S. J. Clark, M. D. Segall, C. J. Pickard, P. J. Hasnip, M. J. Probert, K. Refson, M. C. Payne, *Z. Kristallogr.* **2005**, *220*, 567.

[25] C. J. Pickard, F. Mauri, *Phys. Rev. B* **2001**, *63*, 245101.

[26] J.-P. Amoureux, C. Fernandez, S. Steuernagel, *J. Magn. Reson*. A **1996**, *123*, 116.

[27] K. J. Pike, R. P. Malde, S. E. Ashbrook, J. McManus, S. Wimperis, *Solid State Nucl. Magn. Reson*. **2000**, *16*, 215.

[28] M. Bak, J. Rasmussen, N. Nielsen, *J. Magn. Reson*. **2000**, *147*, 296.

[29] J. P. Perdew, K. Burke, M. Ernzerhof, *Phys. Rev. Lett.* **1996**, *77*, 3865.

[30] J. R. Yates, C. J. Pickard and F. Mauri, *Phys. Rev. B* **2007**, *76*, 024401.

[31] J. R. Yates, C. J. Pickard, M. C. Payne, F. Mauri, *J. Chem. Phys.* **2003**, *118*, 5746.

[32] H. J. Monkhorst, J. D. Pack, *Phys. Rev. B* **1976**, *13*, 5188.

[33] R. Grau-Crespo, S. Hamad, C. R. A. Catlow, N. H. de Leeuw, *J. Phys.: Condens. Matter* **2007**, *19*, 256201.

[34] P. Pyykko, *Mol. Phys*. **2018**, *116*, 1328.

[35] B. C. Chakoumakos, *J. Solid State Chem*. **1984**, *53*, 120.

[36] B. J. Kennedy, *Mater. Sci. Forum* **1996**, *228*, 753.

[37] M. A. Subramanian, G. Aravamudan, G. V. Subba Rao, *Prog. Solid State Chem*. **1983**, *15*, 55.

[38] F. Brisse, O. Knop, *Can. J. Chem.* **1968**, *46*, 859.

[39] R. C. Ewing, W. J. Weber, J. Lian, *Appl. Phys. Rev.* **2004**, *95*, 1.

[40] N. Kim, C. P. Grey, *J. Solid State Chem*. **2003**, *175*, 110.

[41] R. K. Harris, A. C. Olivieri, *Prog. Nucl. Magn. Reson. Spectrosc.* **1992**, *24*, 435.

[42] S. E. Ashbrook, J. McManus, M. J. Thrippleton, S. Wimperis, *Prog. Nucl. Magn. Reson. Spectrosc*. **2009**, *55*, 160.

[43] R. W. Schurko *Acc. Chem. Res.* **2013**, *46*, 1985.

[44] M. Pirzada, R. W. Grimes, L. Minervini, J. F. Macguire, K. E. Sickafus, *Solid State Ionics* **2001**, *140*, 201.

[45] P. J. Wilde, C. R. A. Catlow, *Solid State Ionics* **1998**, *112*, 173.

[46] M. P. van Dijk, A. J. Burggraaf, A. N. Cormack, C. R. A. Catlow, *Solid State Ionics* **1985**, *17*, 159.

[47] R. D. Shannon, *Acta Crystallogr., A* **1976**, *A32*, 751.

[48] A. Fernandes, R. F. Moran, D. McKay, B. Griffiths, A. Herlihy, K. R. Whittle, D. M. Dawson, S. E. Ashbrook, Exploring Cation Disorder in Mixed-Metal Pyrochlore Ceramics using ^{17}O NMR Spectroscopy and First-Principles Calculations. Dataset. University of St Andrews Research Portal. DOI: XXX.

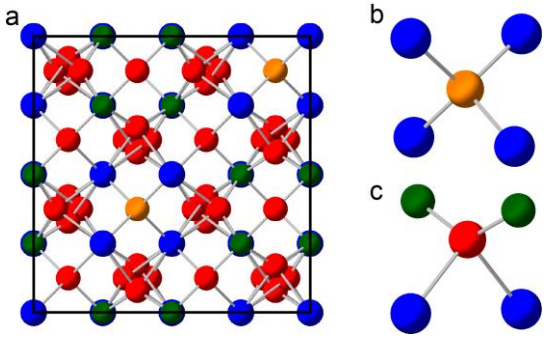

Figure 1. (a) Structure of an $A_2B_2O_7$ pyrochlore, and local environments of (b) O1 (8a) and (c) O2 (48f) sites. Atoms are coloured with A = blue, B = green, O1 = orange and O2 = red.

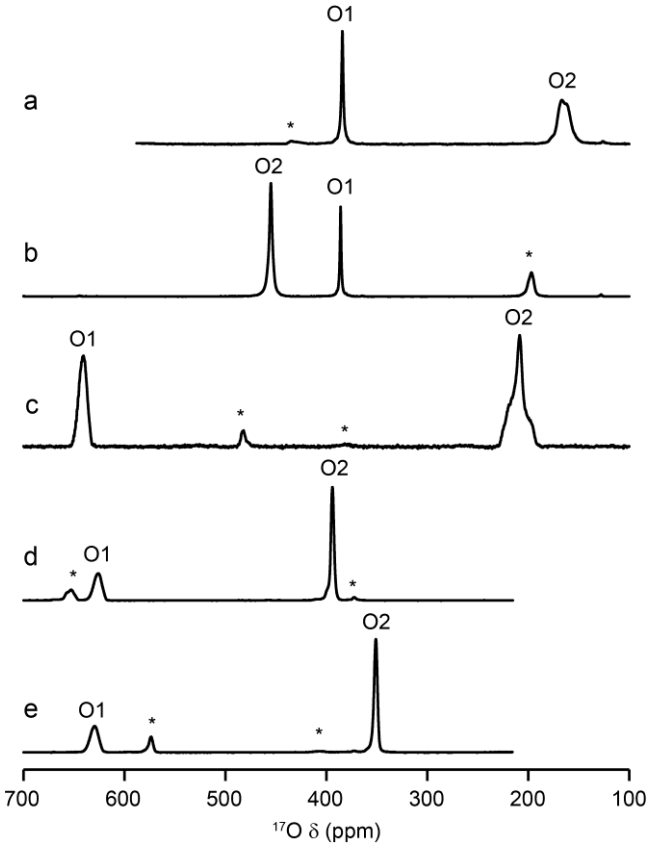

Figure 2. ^{17}O (14.1 T) NMR spectra of (a) $Y_2Sn_2O_7$, (b) $Y_2Ti_2O_7$, (c) $La_2Sn_2O_7$, (d) $La_2Zr_2O_7$ and (e) $La_2Hf_2O_7$. Spectra were recorded with MAS rates of (a-d) 21 kHz and (e) 18 kHz. Spinning sidebands are marked with asterisks (*).

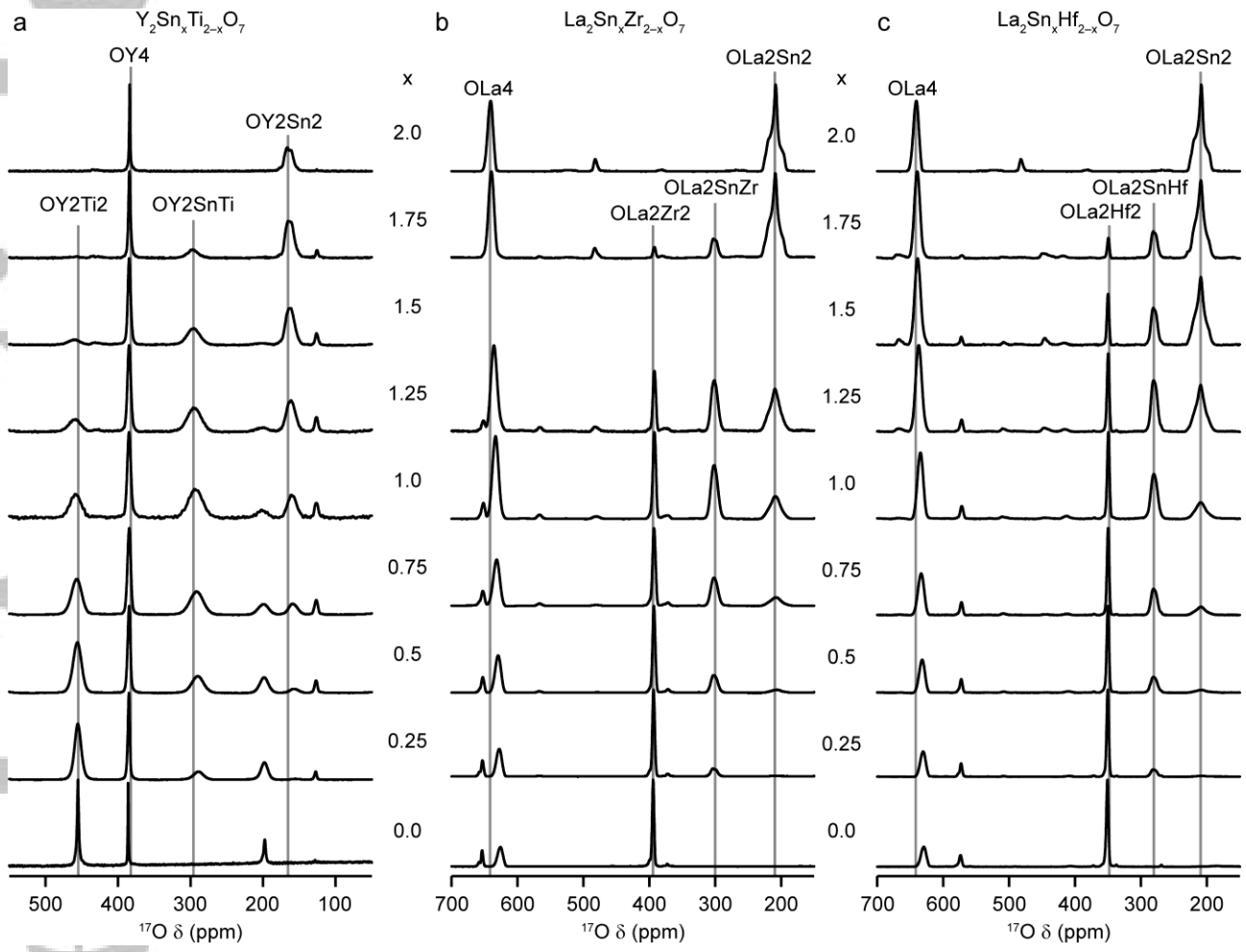

Figure 3. ^{17}O (14.1 T, 21 kHz MAS) NMR spectra of (a) $Y_2Sn_xTi_{2-x}O_7$, (b) $La_2Sn_xZr_{2-x}O_7$ and (c) $La_2Sn_xHf_{2-x}O_7$. Grey vertical lines serve as guides to the eye. All spectra are vertically normalized to the most intense resonance.

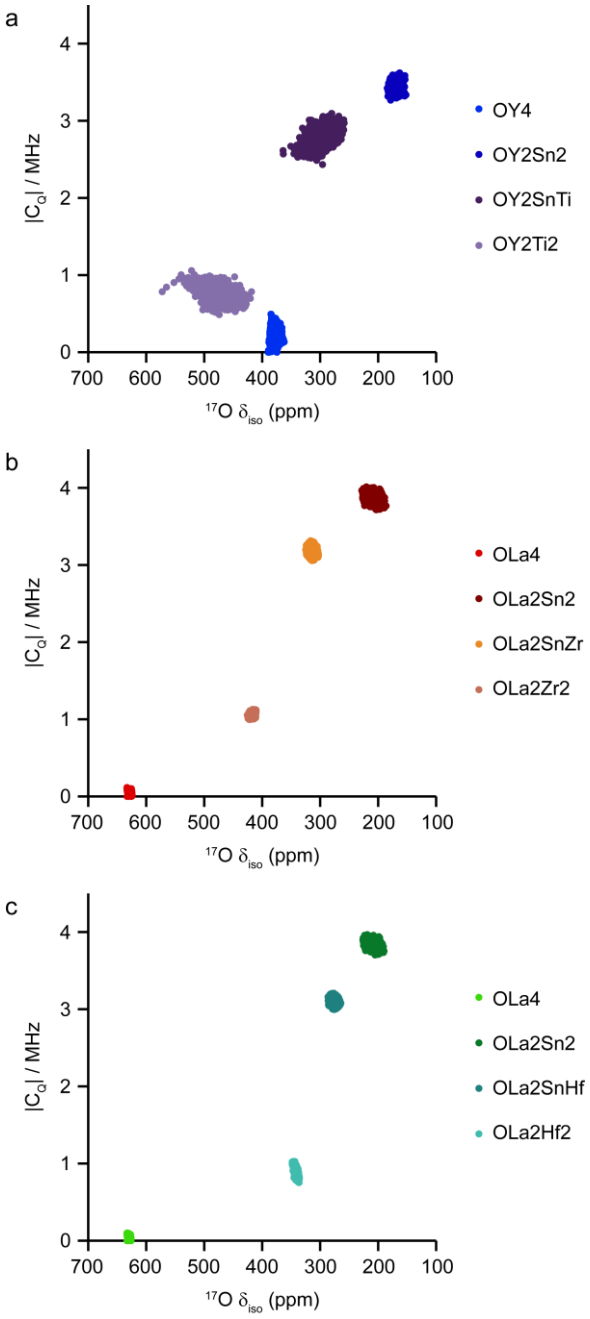

Figure 4. Plots of calculated ^{17}O $|C_Q|$ against δ_{iso} for (a) $Y_2Sn_xTi_{2-x}O_7$, (b) $La_2Sn_xZr_{2-x}O_7$ and (c) $La_2Sn_xHf_{2-x}O_7$.

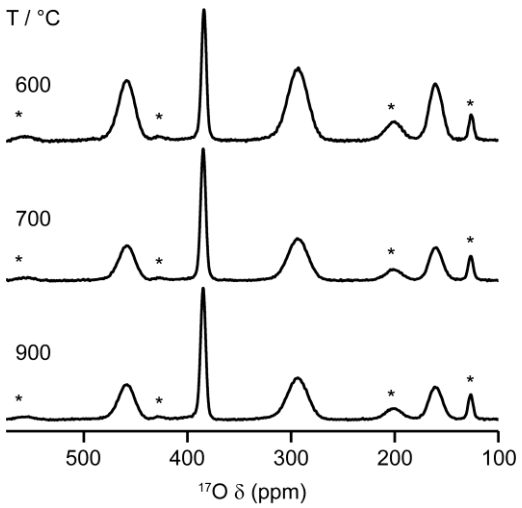

Figure 5. ^{17}O (14.1 T, 21 kHz MAS) NMR spectra of Y_2SnTiO_7 enriched in $^{17}O_2$ gas at the indicated temperatures for 12 h. Asterisks denote spinning sidebands. Spectra are normalized to the most intense resonance.

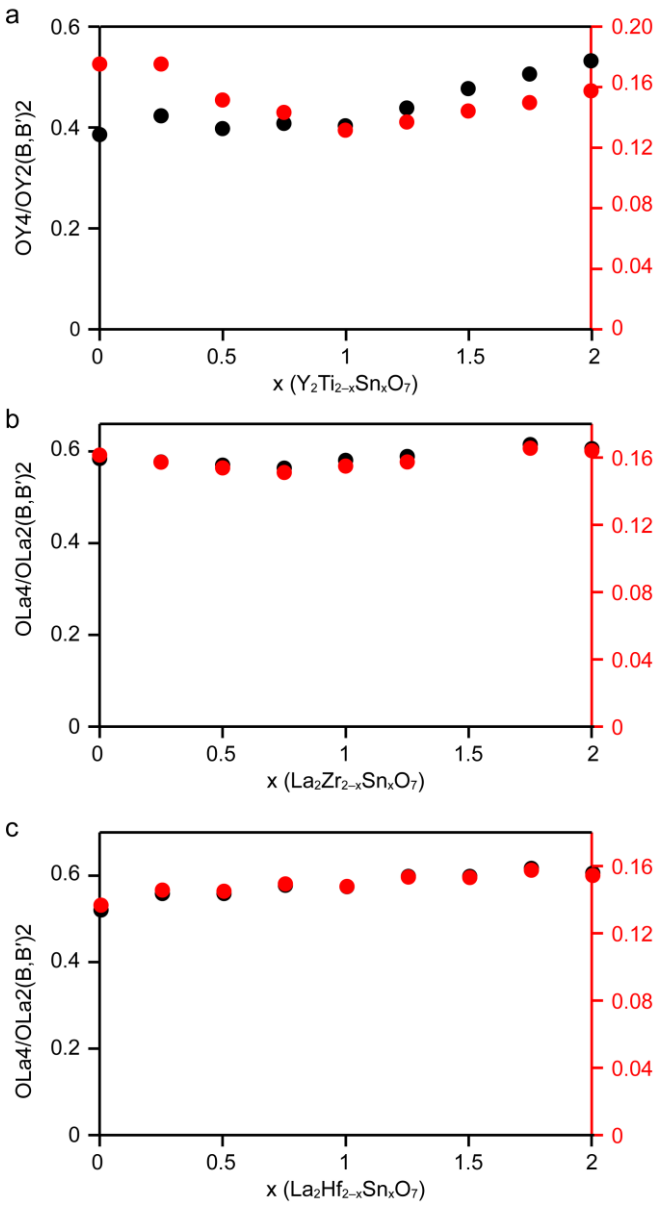

Figure 6. Plots showing the (integrated) intensity ratio, OA4/OA2(B,B′)2, extracted from the ^{17}O MAS NMR spectra of (a) $Y_2Sn_xTi_{2-x}O_7$, (b) $La_2Sn_xZr_{2-x}O_7$ and (c) $La_2Sn_xHf_{2-x}O_7$, enriched at 900 °C for 12 h (shown in Figure 3). Red points and axes correspond to the OA4/OA2(B,B′)2 ratio obtained after correction for the effects of T_1 relaxation and the contribution of the STs.

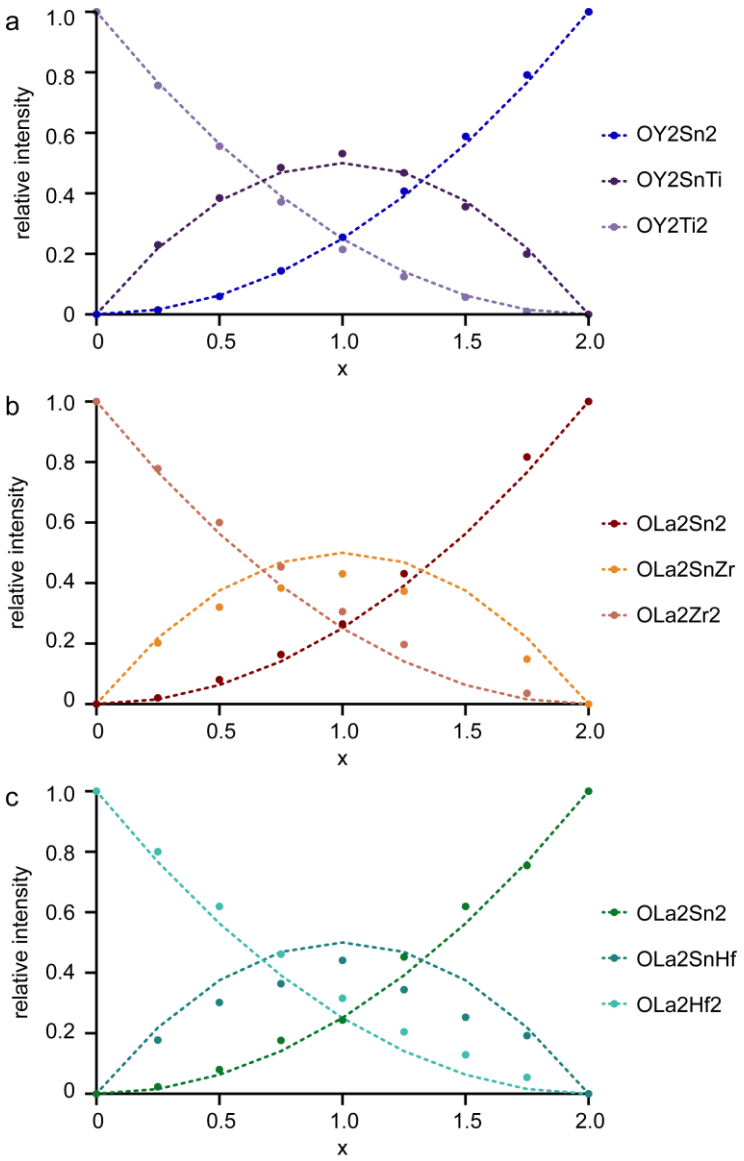

Figure 7. Plots of corrected experimental integrated intensities of OA2B2 signals as a function of x (points) and expected integrated intensities for a random distribution of cations (dashed lines) for (a) $Y_2Sn_xTi_{2-x}O_7$, (b) $La_2Sn_xZr_{2-x}O_7$ and (c) $La_2Sn_xHf_{2-x}O_7$.

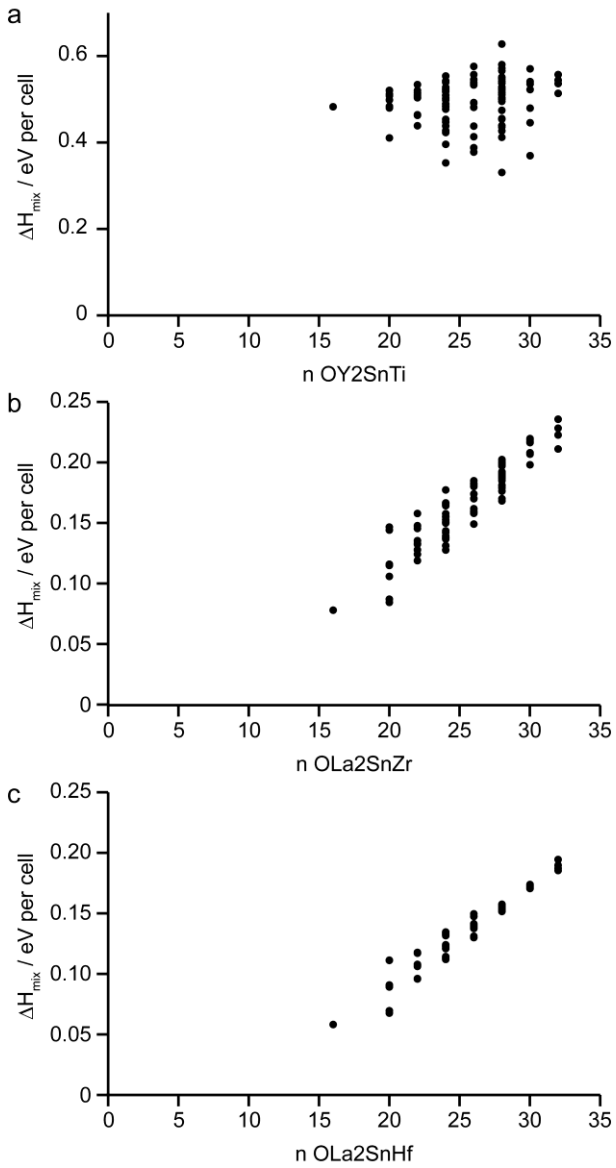

Figure 8. Plots of ΔH_{mix} against number of OA2BB′ species per unit cell for structural models of (a) Y_2SnTiO_7, (b) La_2SnZrO_7 and (c) La_2SnHfO_7.

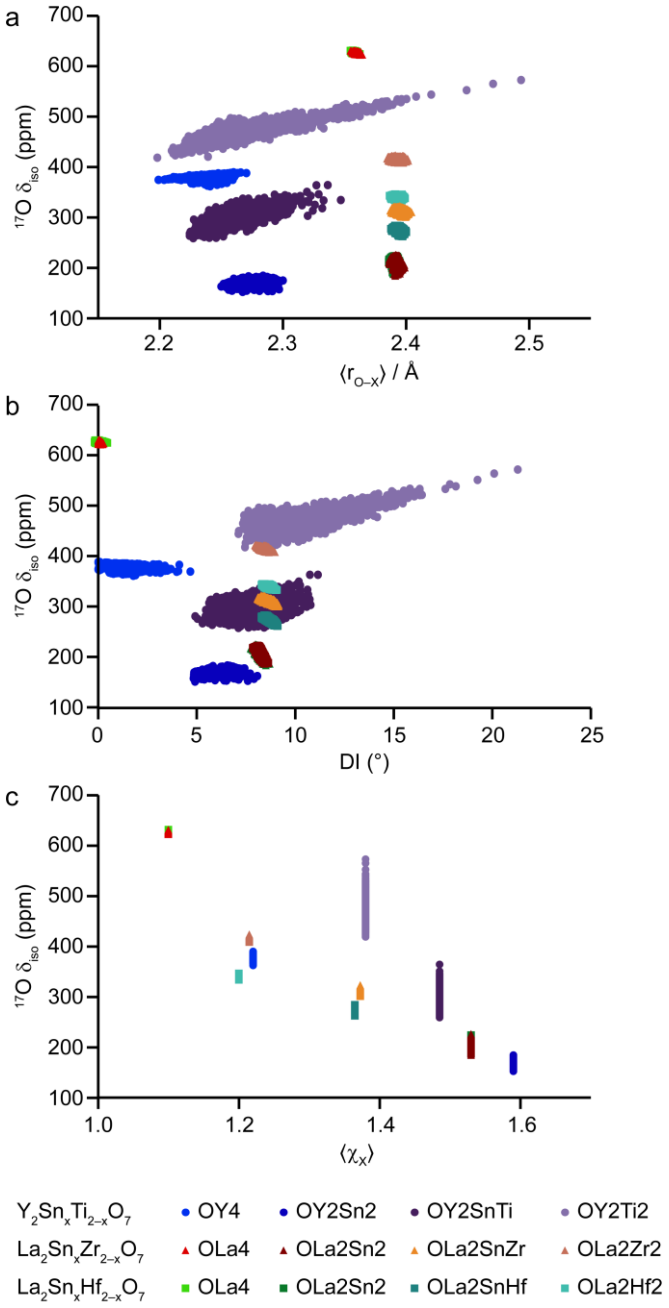

Figure 9. Plots of calculated ^{17}O δ_{iso} against (a) mean O–cation bond length, (b) distortion index of the O tetrahedral site and (c) mean electronegativity of the four surrounding cations for $Y_2Sn_xTi_{2-x}O_7$ (circles) $La_2Sn_xZr_{2-x}O_7$ (triangles) and $La_2Sn_xHf_{2-x}O_7$ (squares).

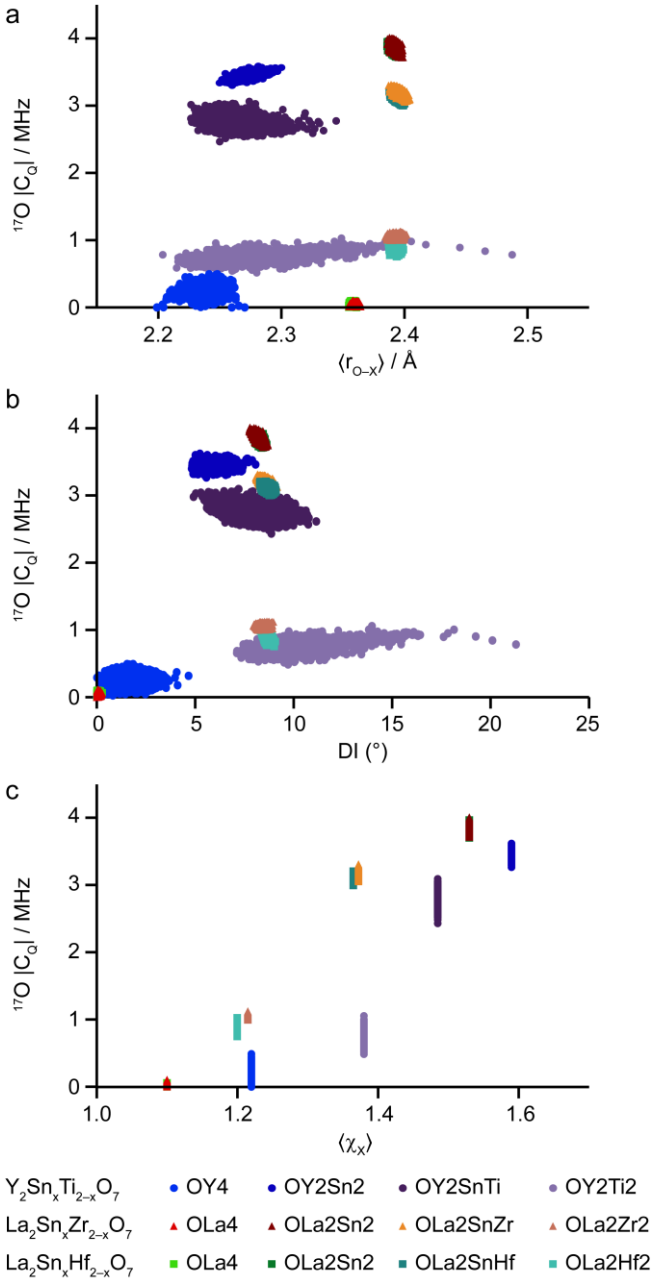

Figure 10. Plots of calculated ^{17}O |C_Q| against (a) mean O–cation bond length, (b) distortion index of the O tetrahedral site and (c) mean electronegativity of the four surrounding cations for $Y_2Sn_xTi_{2-x}O_7$ (circles) $La_2Sn_xZr_{2-x}O_7$ (triangles) and $La_2Sn_xHf_{2-x}O_7$ (squares).

TOC ENTRY

Exploring Cation Disorder in Mixed-Metal Pyrochlore Ceramics using ^{17}O NMR Spectroscopy and First-Principles Calculations

Arantxa Fernandes, Robert F. Moran, David McKay, Ben Griffiths, Anna Herlihy, Karl R. Whittle, Daniel M. Dawson* and Sharon E. Ashbrook*

We combine uniform ^{17}O isotopic enrichment with quantitative ^{17}O NMR spectroscopy and comprehensive computational modelling to investigate cation disorder in the pyrochlore solid solutions, $Y_2Sn_xTi_{2-x}O_7$, $La_2Sn_xZr_{2-x}O_7$ and $La_2Sn_xHf_{2-x}O_7$. We demonstrate that the cation distribution in $Y_2Sn_xTi_{2-x}O_7$ is essentially random, whereas in $La_2Sn_xZr_{2-x}O_7$ and $La_2Sn_xHf_{2-x}O_7$, the more "mixed" OLa2SnZr and OLa2SnHf sites are slightly energetically disfavoured, leading to some deviation from a totally random cation distribution.